Pressure and temperature dependence of interlayer spin diffusion and electrical conductivity in the layered organic conductors κ-(BEDT-TTF)$_2$Cu[N(CN)$_2$]X ($X =$ Cl, Br)

Ágnes Antal,[1] Titusz Fehér,[1] Erzsébet Tátrai-Szekeres,[1] Ferenc Fülöp,[1] Bálint Náfrádi,[1,2] László Forró,[2] and András Jánossy[1,*]

[1]*Budapest University of Technology and Economics, Institute of Physics and Condensed Matter Research Group of the Hungarian Academy of Sciences, P.O. Box 91, H-1521 Budapest, Hungary*

[2]*Institute of Physics of Complex Matter, FBS, Swiss Federal Institute of Technology (EPFL), CH-1015 Lausanne, Switzerland*

A high frequency (111.2–420 GHz) electron spin resonance study of the interlayer spin diffusion is presented in the conducting phases of the layered organic compounds, κ-(BEDT-TTF)$_2$Cu[N(CN)$_2$]X (κ-ET$_2$-X), $X =$ Cl or Br. The interlayer spin cross relaxation time T_x and the intrinsic spin relaxation time T_2 of single layers are measured as a function of temperature and pressure. Spin diffusion is two dimensional in the high temperature bad-metal phase (i.e., electrons are confined to a single molecular layer for longer than T_2). The interlayer electron hopping frequency $\nu_\perp = 1/(2T_x)$ decreases along the bad-metal to Mott insulator crossover and increases along the bad-metal to normal metal (or superconductor) crossover. The density of states (DOS) is determined from a comparison of T_x and the interlayer resistivity. In the bad-metal phase it is four to five times larger than the DOS calculated from the electronic structure neglecting electron correlations. In κ-ET$_2$-X the DOS increases with pressure along the bad-metal to normal metal crossover. Results are compared with predictions of the dynamical mean field theory.

　　　　PACS number(s): 71.30.+h, 71.20.−b, 76.30.−v, 72.25.−b

I. INTRODUCTION

Layered organic conductors, and in particular members of the κ-(BEDT-TTF)$_2$Cu[N(CN)$_2$]X (henceforth κ-ET$_2$-X) family, are strongly interacting electronic systems on the borderline of a metal to insulator transition. In the crystal structure[1,2] (Fig. 1) insulating single-atom-thick Cu[N(CN)$_2$]X, $X =$ Cl or Br polymeric sheets separate the conducting or magnetic ET molecular layers. The narrow, highly anisotropic electronic bands are half-filled with one hole per molecular dimer, ET$_2$. The intermolecular overlap integrals of neighboring molecules within a layer and in-between layers are of the order of $t_\parallel \approx 0.1$ eV and $t_\perp \approx 0.1$ meV, respectively.[3,4] Electric conductivity is two dimensional (2D), the measured anisotropy[5–7] is between 100 and 1000.

At low temperatures, under moderate pressures, a Fermi liquid description is thought to be valid for the in-plane transport. However, the interlayer conductivity is, at most, "weakly coherent," tunneling to the second neighbor layer is already incoherent at low temperatures.[4,8] At higher temperatures the in-plane conductivity is also incoherent: The electronic mean free path is much less than the molecular separations.

The pressure-temperature phase diagram[9–11] is of particular interest. κ-ET$_2$-X is a model system, in which the magnetically ordered and the various conducting phases are reached with relative ease (Fig. 2). The high temperature phase is a bad-metal characterized by a very high resistivity. κ-ET$_2$-Cl at ambient pressures undergoes a Mott-Hubbard metal-insulator transition below 50 K and is a weak antiferromagnet below $T_N = 26$ K (Ref. 12). On the other hand, a bad-metal to normal metal transition takes place below 50 K in κ-ET$_2$-Cl at moderate pressures and in the isostructural κ-ET$_2$-Br. In this case the ground state is superconducting at pressures below 0.5 GPa and a normal metal at higher pressure.

In this paper we report on the interlayer spin diffusion rate in κ-ET$_2$-Br as a function of temperature, and in κ-ET$_2$-Cl, as a function of temperature and pressure, measured by conduction electron spin resonance (CESR) at high magnetic fields. We discuss the relation between electrical conductivity and spin diffusion. The method makes use of the alternating sandwich structure of κ-ET$_2$-X and is not applicable to all layered systems. Nevertheless, with the availability of highly sensitive high frequency electron spin resonance (ESR0 spectrometers many more interesting systems can be studied. There are a large number of organic crystals with alternating molecular layers or chains. Using the method, magnetic interactions between quasi-one-dimensional molecular chains were measured by Cabanas and Schwerdtfeger.[13] Very small interactions are measurable (e.g., in the antiferromagnetic phase of κ-ET$_2$-Cl an interlayer effective magnetic field of 1 mT was found[14]). This value is several orders of magnitude smaller than exchange fields within a single layer.

We find spin diffusion is 2D in κ-ET$_2$-X at high temperatures with a crossover to three dimensional (3D) in the metallic compounds at lower temperatures. In quasiclassical models, spin and charge transport between metallic layers are proportional. Indeed, the temperature and pressure dependence of the interlayer spin hopping rate and the interlayer conductivity is similar, differences are attributed to changes in the density of states (DOS).

The paper is organized as follows. Following a brief description of the experimental setup and samples (Sec. II) we detail in Sec. III the method used to determine the interlayer coupling parameters. Section IV is devoted to the experimental results, we present the spin hopping (or cross-relaxation) times between layers T_x and the intrinsic spin lifetime of individual layers T_2. In Sec. V we compare the spin hopping time and the resistivity. A short account of the method was published in Ref. 15.
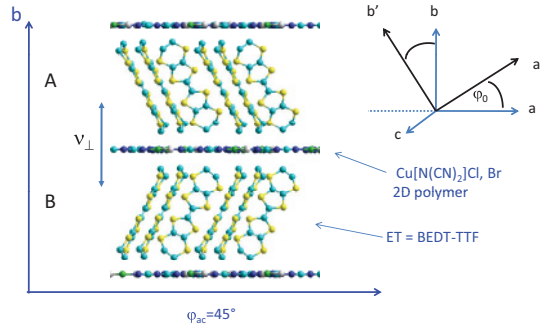
FIG. 1. (Color online) Structure of κ-ET$_2$-Cl and κ-ET$_2$-Br. Conducting ET [bis(ethylenedithio)-tetrathiafulvalene] layers are separated by insulating Cu[N(CN)$_2$]X, X = Cl or Br polymeric layers. $\nu_\perp$ is the interlayer electron hopping rate measured by ESR. The Larmor frequencies of chemically equivalent A and B layers are different in general orientation magnetic fields. φ_{ac} is the angle from a in the (a,c) plane. φ_0 is the orientation of the g tensor principal axes a', b' of layer A.

II. EXPERIMENTAL METHODS

κ-ET$_2$-Cl and κ-ET$_2$-Br single crystals with typical dimensions of $1 \times 1 \times 0.2$ mm^3 were grown by standard electrochemical methods in Ar gas filled electrolytic cells. The electrolytic cell was placed in an additional temperature regulated argon gas chamber to prevent oxygen and water contamination. The quality of several single crystals was verified by x-ray diffraction.

The high frequency ESR spectrometers at the Swiss Federal Institute of Technology (EPFL) (210, 315, and 420 GHz) and the Budapest University of Technology and Economics BUTE (111.2 and 222.4 GHz) have similar designs.[16–18] A nonresonant mm-wave circuit allows for the *in situ* change of the frequency and rotation of the crystal around a single axis. A Daphne 7373 oil filled clamp pressure cell was used. The pressures quoted are nominal values at 300 K; the pressure loss between 300 and 4 K is about 0.2 GPa. The sample cooling rate was 1 K/min or slower. Some samples were warmed and
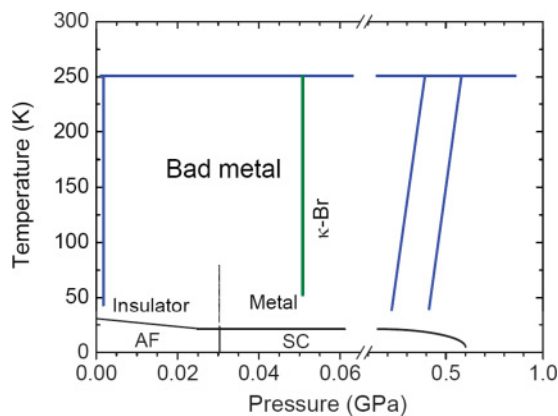

FIG. 2. (Color online) Schematic pressure-temperature phase diagram of κ-ET$_2$-Cl. ESR experiments on κ-ET$_2$-Cl were along the thick lines. The κ-ET$_2$-Br ESR experiment line at ambient pressure is marked at 50 MPa to take into account the "chemical pressure."

cooled several times, but there was no thermal or magnetic field history dependence in the ESR spectrum.

Four probe dc conductivity measurements in the highly conducting planes were done with gold contacts attached to the thin crystal surfaces. The temperature sweeps deteriorated the contacts and the first down sweep data are reported.

III. MEASUREMENT METHOD OF INTERLAYER SPIN DIFFUSION AND EXCHANGE FIELDS

Weak interactions between magnetic subsystems or sublattices can be precisely measured from an analysis of the ESR spectrum[19] whenever there are at least two weakly interacting magnetic sublattices with different Larmor frequencies. Here we apply the method to measure the magnetic interactions, the hopping rate and exchange fields, between adjacent chemically equivalent, but crystallographically inequivalent ET molecular layers in the paramagnetic phases of κ-ET$_2$-X, X = Br, and Cl. The weakly ferromagnetic phase of κ-ET$_2$-Cl was discussed in Ref [14].

The orthorhombic crystal structure of κ-ET$_2$-X (Refs. [1,2]) can be looked upon as a sandwich of two monoclinic crystals (Fig. [1]) in which the orthogonal a and c axes coincide while the b_A and b_B axes of the A and B layers are tilted from the orthorhombic b axis. The conducting ET layers are separated by a single-atom-thick Cu[N(CN)$_2$]X "insulating" polymeric layer. The interaction between the layers is determined from the mixing of the ESR spectra of the separate layers. The interlayer hopping times are between 10^{-10} s and 10^{-8} s; this interaction is weak, but essential for the understanding of the electronic and magnetic properties.

To calculate the ESR spectrum, we assume that spin diffusion from the adjacent B layers increases the magnetization of layer A, $\boldsymbol{M}^A$, with a rate of $(\boldsymbol{M}^B - \boldsymbol{M}^A)/T_x$ and $\boldsymbol{M}^B$ exerts a torque on $\boldsymbol{M}^A$ with an effective magnetic field $\lambda\boldsymbol{M}^B$. Similar expressions describe the effect of A layers on B. The ESR spectrum (i.e., the dynamic susceptibility) is given by two coupled Bloch equations where the torque of the external static and exciting magnetic fields and the intrinsic spin relaxation are added. For layer A the equation of motion of the $j = x,y$ components perpendicular to the static field are

$$\frac{dM_j^A}{dt} = [\gamma^A \boldsymbol{M}^A \times (\lambda \boldsymbol{M}^B + \boldsymbol{B})]_j - \frac{M_j^A}{T_{2A}} + \frac{M_j^B - M_j^A}{T_x}. \quad (1)$$

The coupled Bloch equations were solved numerically to obtain the absorption spectrum, $G(B)$ as a function of the external magnetic field magnitude B for fixed excitation frequency. The single layer parameters g_A, g_B, T_{2A}, T_{2B} (or the average T_2), and the interaction parameters λM_0 and T_x are obtained from a best fit to the experiment (M_0 is the magnitude of the static magnetization, $g_A = \gamma^A \hbar/\mu_B$ is the gyromagnetic tensor). In principle all parameters can be determined from the spectrum at a single exciting frequency and sweeping the external field. Nevertheless, the experiments were, in most cases, done at two or more frequencies to make the least-squares optimization of the model parameters to the measured spectra more stable.

If the line separation is much larger than the interlayer interaction, the spectrum consists of two Lorentzian lines with Larmor frequencies

$$\nu_{A,B} = \frac{\mu_B}{h}|g_{A,B}\boldsymbol{B}|. \tag{2}$$

The exchange field and cross relaxation have very different effects on the ESR spectrum. In conductors the cross relaxation dominates over the exchange fields and the lines coalesce when

$$|\nu_A - \nu_B| \approx \frac{1}{T_x}. \tag{3}$$

The interaction parameters are the most precisely determined when this condition is fulfilled. The spectrum is symmetric around the average of the two Larmor frequencies at all values of $1/T_x$ if $\lambda = 0$ and $T_{2A} = T_{2B}$.

On the other hand, if $\lambda \neq 0$ (i.e., when magnetic coupling between layers is important) the absorption spectrum $G(B)$ is asymmetric. For an antiferromagnetic coupling ($\lambda < 0$), the higher field resonance loses intensity to the lower field one. Cabanas and Schwerdtfeger[13] noticed this curious behavior in the ESR of an insulating quasi-one-dimensional (1D) organic crystal with weakly interacting inequivalent paramagnetic chains.

IV. EXPERIMENTAL RESULTS

A. g factor anisotropy

The g factor anisotropy of κ-ET$_2$-Cl and κ-ET$_2$-Br at high magnetic fields, ($\nu_L = 222.4$ GHz, $B \approx 8$ T) has the usual sinusoidal form. There is a single line in the (a,c) and (b,c) planes. The lines of the A and B layers are well resolved in the (a,b) plane (Fig. 3). The interactions between the layers affect little (although measurably) the 222.4 GHz ESR spectrum and the g factors listed in Table I were obtained by fitting two equal intensity Lorentzians with unequal line widths $1/(\gamma_A T_{2A})$ and $1/(\gamma_B T_{2B})$. Measurements at 111.2 GHz confirmed that the
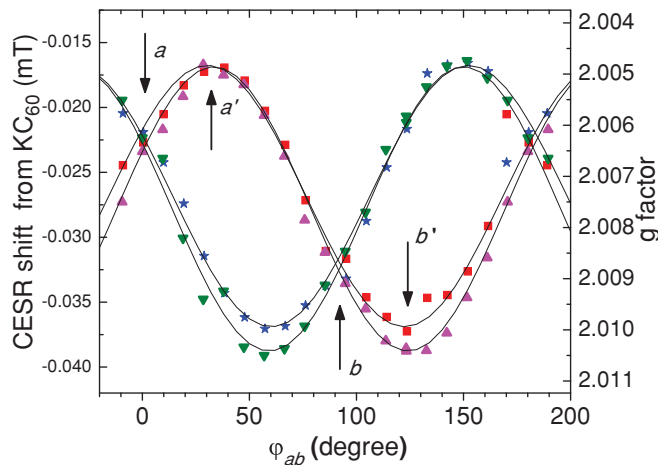

FIG. 3. (Color online) g factor anisotropies in the (a,b) plane measured at 222.4 GHz and 250 K. κ-ET$_2$-Cl: red squares, ■ and blue stars, ∗. κ-ET$_2$-Br: magenta triangles up, ▲; green triangles down, ▼. a' and b' denote g factor principal axes of A layers (see Fig. 1), a and b are the orthorhombic lattice directions. Lines are fits with parameters in Table I.

TABLE I. Principal values of the g tensor in κ-ET$_2$-X.

X	T	g'_a	g'_b	$g'_c = g_c$	g_a	g_b
Cl	45 K	2.0047	2.0098	2.0048	2.0065	2.0081
	250 K	2.0048	2.0099	2.005	2.0061	2.0086
Br	45 K	2.0044	2.0097	2.0049	2.0064	2.0082
	250 K	2.0048	2.0102	2.0049	2.0064	2.0088
Br(9 GHz)[a]	300 K	n.a.	n.a.	2.0048	2.0063	2.0088

[a]The Br g factors at 300 K were measured by Nakamura *et al.* (Ref. 20) at 9 GHz.

g factors derived from the 222.4 GHz data are to a good approximation equal to the g factors of independent layers.

The principal directions of the g factor tensors are rotated about the c axis by $\varphi_0 = 32° \pm 5°$ (29° ± 5°), from the orthorhombic a axis for $X = $ Cl (Br). We estimate an error of ±0.0002 in the g factors from a ±5° alignment uncertainty and the uncertainty in $g_{KC_{60}} = 2.0006 \pm 0.0001$ of the polymeric KC$_{60}$ reference. The g tensor depends mostly on the ET molecular properties[20] and little on temperature.

Nakamura *et al.*[20] reported the g factor anisotropy of κ-ET$_2$-Br at 9 GHz. At this low frequency a "motionally narrowed" ESR line appears and the g tensor principal directions are along the orthogonal axes. The g factor is independent of frequency between 9 and 222.4 GHz in κ-ET$_2$-Br in contrast with the organic conductor EDT-TTF-CONMe$_2$Br where a nonlinearity in the g factor was attributed to the Dzyaloshinskii-Moriya interaction.[21]

B. Pressure dependence in the bad-metal phase

At high temperatures, roughly above 50 K, κ-ET$_2$-X is in a bad-metal phase, where the in-plane conductivity is low and the in-plane mean free path is less than typical intermolecular distances. The conductivity increases with pressure.[10,22] A comparison of the interlayer spin hopping rate and electronic conductivity[10,22] is the aim of the experiment.

The ESR spectra of a κ-ET$_2$-Cl single crystal were recorded at 250 K as a function of pressure between 0 and 1.06 GPa at 210, 315, and 420 GHz. The crystal was oriented with magnetic field along $\varphi_{ab} \approx 45°$ in the (a,b) plane where the difference between the Larmor frequencies of the A and B layers is about the largest (Fig. 3). The narrow AFMR lines in the antiferromagnetic phase[14] are an indication of the high quality of the crystal. The pressure was changed at ambient temperature in 40 MPa steps. Some of the measured and calculated spectra are displayed in Fig. 4. A Lorentzian ESR line with pressure independent position and width from impurities in the pressure cell was subtracted. The signal to noise ratio depends on pressure dependent variations of standing waves within the cell. The temperature dependence of the ESR measured at various fixed pressures is discussed in the following section. The ESR spectrum was independent of thermal or pressure history, unlike the resistance, which depends on the quality of fragile contacts.

Figure 4 shows the merger of the A and B layer lines as the interlayer hopping rate $1/T_x$ increases with pressure. The spectra calculated using Eq. (1) are almost indistinguishable from the measured spectra. In the calculation the g factors
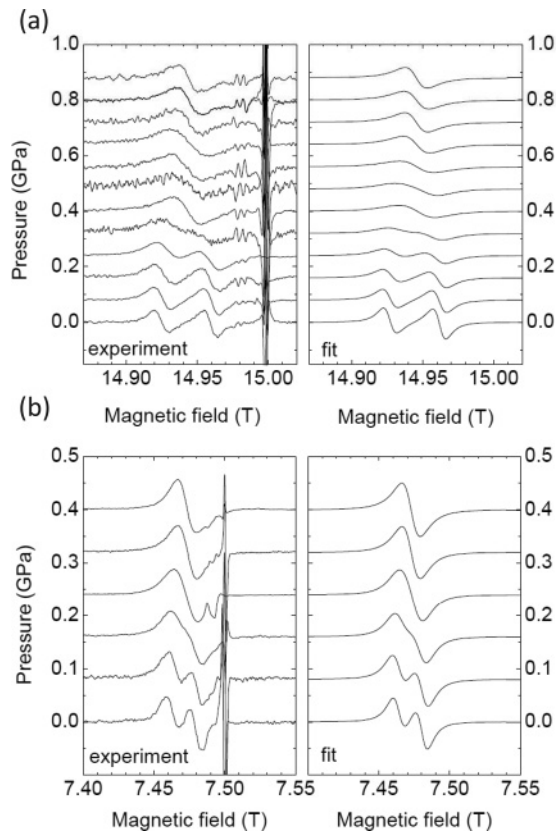
FIG. 4. ESR spectra of κ-ET$_2$-Cl as a function of pressure at 250 K. (a) $\nu_L = 420$ GHz, (b) $\nu_L = 210$ GHz. **B** oriented along $\varphi_{ab} \approx 45°$. Left panels: Experimental spectra. Right panels: Best fit calculated spectra. Note the coalescence of A and B layer ESR lines with increasing pressure. The strong line at 15.00 T (7.50 T) is the KC$_{60}$ reference. An instrumental impurity line at 14.98 T (7.49 T) was subtracted at 420 GHz (210 GHz). This and similar later figures are 2D projections of 3D (magnetic field, pressure, ESR signal) maps.

were assumed to be pressure independent. We assumed layer independent relaxation rates, $T_{2A} = T_{2B} = T_2$, although a small difference between T_{2A} and T_{2B} would be probably more realistic. The determination of T_x is most precise in the range where $|\nu_A - \nu_B| \approx 1/T_x$; at 0.16 and 0.32 GPa for 210 and 420 GHz, respectively.

As shown in Fig. 5, T_x, the cross relaxation time decreases by a factor of 20 while the intrinsic relaxation time T_2 decreases smoothly by a factor of 2 between ambient and 0.94 GPa pressures.

C. Bad-metal to normal metal crossover

κ-ET$_2$-Br at ambient pressure and κ-ET$_2$-Cl under pressure undergo a continuous transition from a bad-metal phase at ambient temperatures to a normal metal phase at low temperatures. κ-ET$_2$-Br has a superconducting ground state and is similar to κ-ET$_2$-Cl under a weak "chemical pressure" equivalent to about 50 MPa. κ-ET$_2$-Cl has a superconducting ground state at pressures between 30 and 500 MPa (Ref. 23).

The crossover was observed in the ESR spectra as a function of temperature in three κ-ET$_2$-Br crystals at ambient pressure and a κ-ET$_2$-Cl crystal at nominally $p = 0.4$ and 0.64 GPa
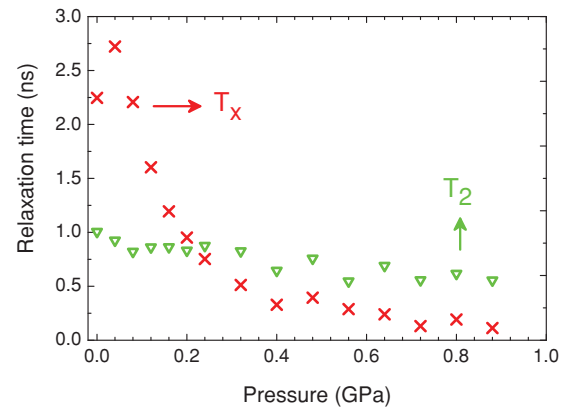

FIG. 5. (Color online) Interlayer cross relaxation time T_x and intrinsic relaxation time T_2 as a function of pressure at 250 K in κ-ET$_2$-Cl determined from the fit to the ESR spectra in Fig. 4. The crossover between 2D and 3D spin diffusion is at 0.2 GPa.

pressures. In the κ-ET$_2$-Br crystals the ESR changes little between 250 and 75 K. Below 50 K, the interlayer hopping rate increases and the A and B layer lines merge rapidly (Fig. 6). There is a qualitative difference between the 250 K pressure dependent crossover in κ-ET$_2$-Cl and the temperature dependent crossover in κ-ET$_2$-Br (Figs. 4 and 6). In both cases the two lines of the A and B layers merge into a single line with the increase of interlayer interactions. However, while in κ-ET$_2$-Cl all spectra are approximately symmetric, in κ-ET$_2$-Br the high field line loses intensity as the temperature is decreased below 50 K. Thus, as explained in Sec. III, the crossover in κ-ET$_2$-Br involves an effective antiferromagnetic field λM_0 between molecular layers in addition to the cross relaxation.

T_x, T_{2A}, T_{2B}, and λM_0 between 40 and 250 K in κ-ET$_2$-Br are shown in Fig. 7. In the fits, g_A was left free to account for its temperature dependence while the difference $g_A - g_B$ was fixed for all temperatures. The exchange field between layers, proportional to the external field, is surprisingly large.
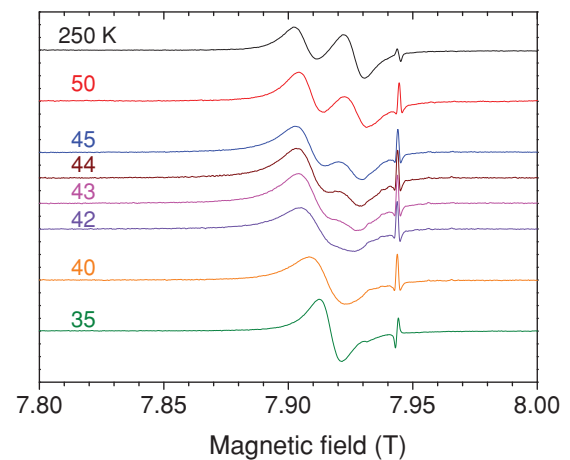

FIG. 6. (Color online) κ-ET$_2$-Br ESR spectra at 222.4 GHz as a function of temperature. **B** is oriented along $\varphi_{ab} \approx 45°$. The A and B layer lines merge at the bad-metal to metal transition between 45 and 40 K. Note the asymmetry of the spectrum above 42 K due to interlayer exchange.
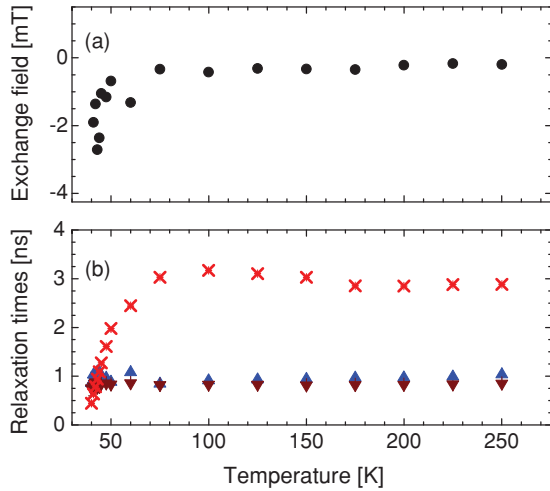
FIG. 7. (Color online) Relaxation times and exchange field in κ-ET$_2$-Br *versus* temperature calculated from the 222.4 and 111.2 GHz ESR spectra. (a) Interlayer exchange field λM_0 at 8 T field (see text). (b) Interlayer cross relaxation T_x (red crosses), intrinsic spin relaxations, T_{2A} (triangles up), and T_{2B} (triangles down). The shortening of T_x below 75 K marks the onset of the bad-metal to normal metal crossover. The 2D to 3D spin diffusion crossover is at 40 K.

$\lambda M_0 = 4$ mT at 222.4 GHz and 40 K is larger than the 1 mT (magnetic field independent) coupling between layers in the antiferromagnetic state of κ-ET$_2$-Cl (Ref. 14).

An enhancement of the interlayer spin diffusion with decreasing temperature has been observed in the κ-ET$_2$-Cl sample under pressures of 0.4 and 0.64 GPa. In these cases the hopping rate is fast, the g factor anisotropy is insufficient to resolve the lines of layers A and B, and T_x was determined from an analysis based on Eq. (1) of the 420 GHz spectra. T_2 was assumed temperature independent and was estimated from an extrapolation of the 250 K linewidths at 210 and 420 GHz to zero frequency. In spite of the uncertainties in the procedure, the decrease of T_x with decreasing temperature (Fig. 8) in this pressure range was unambiguously confirmed.
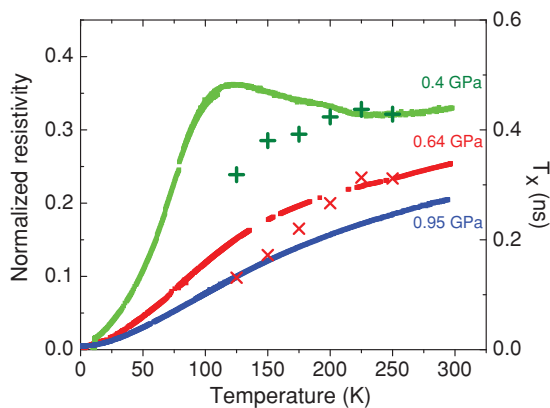

FIG. 8. (Color online) Comparison of the cross relaxation T_x (+ : 0.4 GPa, ×: 0.64 GPa) and the in-plane electrical resistivity (lines) in κ-ET$_2$-Cl under pressure. $\rho_\parallel$ is normalized to the zero pressure resistivity at 250 K. The pressure drops similarly for T_x and $\rho_\parallel$ by about 0.2 GPa between 300 and 4 K.
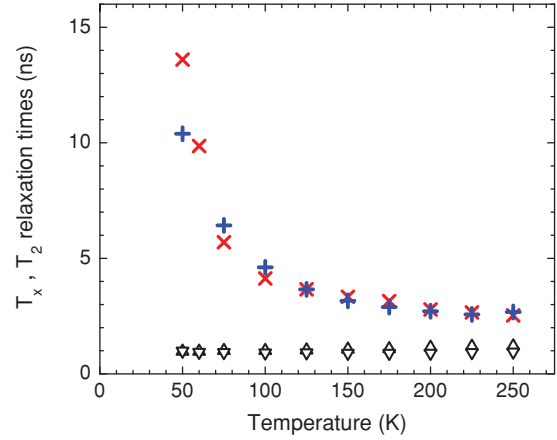

FIG. 9. (Color online) Temperature dependence in κ-ET$_2$-Cl of the spin cross relaxation, T_x (two samples: red × and blue +) and the intrinsic spin relaxation times, T_{2A} (up triangles) and T_{2B} (down triangles). The increase of T_x follows the bad-metal to insulator transition.

D. Bad-metal to insulator transition

κ-ET$_2$-Cl has a continuous metal to insulator transition as the temperature decreases from 300 K to the Néel temperature at 26 K. The lengthening of the interlayer hopping time between 250 and 50 K was measured by ESR at 111.2 and 222.4 GHz on several crystals with consistent results (Fig. 9). The continuous transition to the insulating state is accompanied by the increase of T_x. At 250 K T_x is nearly the same in κ-ET$_2$-Cl and κ-ET$_2$-Br in spite of the insulator and superconductor ground states. The behavior is, however, markedly different below 250 K: In the Br compound T_x is nearly T independent, while it increases rapidly in the Cl compound. The intrinsic spin relaxation T_2 is approximately temperature independent above 50 K. A discussion of the complex behavior between 26 and 50 K (not shown) is deferred to a later publication. In this temperature region two- and three-dimensional magnetic fluctuations play an important role.

V. SPIN DIFFUSION AND ELECTRICAL CONDUCTIVITY

A. Interlayer electron hopping and spin diffusion

The measurement of the interlayer charge hopping frequency $\nu_\perp$ is the most important result of this paper. We define $\nu_\perp$ as the charge hopping frequency through a *single* polymeric barrier and assume

$$\frac{1}{T_x} = 2\nu_\perp, \tag{4}$$

where T_x describes spin diffusion to the two neighboring molecular layers. Strictly speaking, Eq. (4) is not always valid; spin cross relaxation can arise without charge transfer and charge transport is not necessarily accompanied by spin diffusion. Near the superconducting transition temperature, fluctuating electron pairs tunneling between layers contribute to charge transport but not to the spin transport. However, at temperatures well above the antiferromagnetic Néel temperature or the superconducting transition temperature the quasiclassical electron diffusion model is applicable (i.e.,

interlayer spin and charge diffusion are tied together if one assumes that magnetic and superconductor correlations are unimportant).

Tunneling between molecular layers and phonon assisted hopping over the barrier of the insulating polymeric layer determine the hopping frequency $\nu_\perp$. In κ-ET$_2$-Cl at ambient pressure phonon assisted hopping probably dominates $\nu_\perp$ between 50 and 300 K as it increases roughly exponentially with increasing temperature. In κ-ET$_2$-Cl under pressure and in κ-ET$_2$-Br, $\nu_\perp$ increases or is constant with decreasing temperature thus tunneling through the barrier is the dominant mechanism for the interlayer transport.

In an attempt to explain the temperature and frequency dependence of the conductivity anisotropy in κ-ET$_2$-Br, McGuire *et al.*[8] proposed a leakage contribution to the interlayer conductivity through a low concentration of defect holes in the polymeric layers. In the analysis of ESR spectra this sample dependent effect was not taken into account.

B. Comparison of interlayer spin diffusion and electrical conductivity

In the metallic phase, $\nu_\perp$ is closely related to the interlayer electrical resistivity $\rho_\perp$. If the electrons of molecular layers form a Fermi liquid then the interlayer conductivity calculated from the spin hopping rate is[24]

$$\rho_{\perp s}^{-1} = e^2 g(E_F) \nu_\perp d / F, \tag{5}$$

where $g(E_F)$ is the DOS per ET dimer for both spin directions of the metallic layers at the Fermi energy, E_F. $1/F$ is the two-dimensional charge carrier density; in κ-ET$_2$-X $F = (ac)/2$. Here a and c are the in-plane and $b = 2d$ the out-of-plane lattice constants. The significance of Eq. (5) lies in the possibility to determine the DOS from measurements of the conductivity and spin diffusion.

In the bad-metal phase of κ-ET$_2$-X the concept of a DOS at a well-defined Fermi energy fails. The uncertainty due to the momentum lifetime $\hbar/\tau$ is comparable to E_F and Eq. (5) is only approximately valid with $g(E_F)$ replaced by an average DOS. In a two-dimensional free electron gas $g(E)$ is constant and this justifies the use of $g(E_F)$ calculated for noncorrelated metals for comparison with the DOS extracted from the experiment.

The DOS is obtained from Eq. (5) using T_x measured in the present work and typical $\rho_\perp$ values reported in the literature. T_x at zero pressure and 250 K in two κ-ET$_2$-Cl samples is 2.6 ± 0.5 ns and 2.6 ± 1 ns, respectively. In a κ-ET$_2$-Br crystal $T_x = 2.9 \pm 0.5$ ns, within experimental uncertainty the same value as in κ-ET$_2$-Cl. The systematic uncertainties of the fits are the main source of errors. Using the DOS, $g(E_F) = 4.4$ states/eV per two ET and two spins from the noncorrelated electronic structure calculations of Ref. 25, the ambient temperature, zero pressure interlayer resistivity estimated from Eq. (5) is $\rho_{\perp s} = 2.7$ Ωm (3.0 Ωm) in κ-ET$_2$-Cl (κ-ET$_2$-Br).

On the other hand, resistivities of $\rho_\perp = 0.4$–0.5 Ωm for κ-ET$_2$-Br (Refs. 5,26) and $\rho_\perp = 0.9$ Ωm for κ-ET$_2$-Cl (Ref. 6) at 300 K were reported. To satisfy Eq. (5) with the above T_x and $\rho_\perp$ values, the DOS of the correlated electron system has to be about 20 states/eV per two ET. Electron susceptibility and specific heat[25] and cyclotron frequency[27] measurements

imply that at low temperatures the DOS is two to three times higher than predicted by band structure calculations. In our measurements, performed in the high temperature bad-metal phase, a factor of 4–5 larger DOS is needed to satisfy Eq. (5).

Equation (5) is valid for both tunneling and phonon assisted hopping over the barrier. In both κ-ET$_2$-Br and κ-ET$_2$-Cl at ambient pressure the magnetic susceptibility and thus the DOS is nearly temperature independent[28,29] between 50 and 300 K. In both compounds the similar temperature dependence of T_x and $\rho_\perp$ predicted by Eq. (5) is approximately followed in this temperature range. In κ-ET$_2$-Br the interlayer transport is dominated by tunneling. T_x is nearly constant between 250 and 100 K and decreases abruptly below 100 K, signaling the bad-metal to Fermi liquid transition. The temperature dependence of T_x and $\rho_\perp$ (Refs. 5 and 26) is similar but not precisely the same as there is some variation in the reported $\rho_\perp(T)$. A maximum above the metal to bad-metal crossover reported by Buravov[5] and in some crystals by Strack *et al.*[26] does not appear in the T_x data.

Phonon assisted hopping is a natural explanation for the rapid increase of T_x below 300 K. Another possibility is that electrons are gradually localized as the Mott-Hubbard metal-insulator transition is approached and the interlayer hopping decreases together with the in-plane conductivity (see Sec. V E). In κ-ET$_2$-Cl at ambient pressure, between 300 and 50 K, the increase in T_x is similar to the resistivity measured in Ref. 6.

The pressure dependence of T_x in κ-ET$_2$-Cl at 250 K is compared with the pressure dependence of $\rho_\perp$ measured by Weiss *et al.*[22] at 300 K in Fig. 10. According to Eq. (5), the increase of $\rho_\perp/T_x$ by a factor of about 3 with increasing pressure from 0 to 1 GPa signals a strong decrease of the DOS as the material changes from a bad-metal toward a normal metal phase. We discuss the relevance of this effect to theoretical models in Sec. V D.

C. In-plane conductivity in the bad-metal phase

The in-plane resistivity, $\rho_\parallel$ of a κ-ET$_2$-Cl crystal from the same batch as the crystal used for the pressure dependent ESR was measured at 300 K as a function of pressure (Figs. 8 and 10). The temperature dependence of $\rho_\parallel$ was measured at
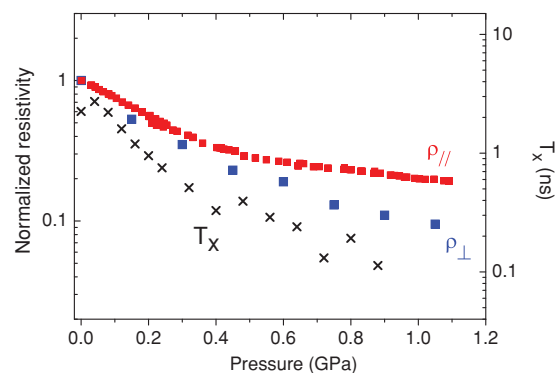

FIG. 10. (Color online) Comparison of the cross relaxation T_x to the interlayer resistivity $\rho_\perp$ (data of Weiss *et al.*[22]), and in-plane resistivity $\rho_\parallel$ (present work) in κ-ET$_2$-Cl *versus* pressure. Resistivity data are normalized at zero pressure.

pressures of 0.4, 0.64, and 0.96 GPa. The temperature and pressure dependence of T_x follows roughly $\rho_\parallel$ (Figs. 8, 9, and 10) normalized to the $P = 0$ GPa, 250 K value.

Above 50 K, $\rho_\parallel$ is extremely large in κ-ET$_2$-X, typically 10^{-2} to 10^{-3} Ωm (Refs. 5 and 6). To appreciate how large $\rho_\parallel$ is, we compare it to the resistivity $\rho_{2D} = 2\pi\hbar d/(e^2 k_F \lambda_c)$ of a 2D system with a free electron band structure. The Ioffe-Regel condition (i.e., a mean path equal to the molecular distance, $\lambda_c = a_0$) gives an upper limit for the metallic resistivity in many conductors.[30] In κ-ET$_2$-Br the Ioffe-Regel condition corresponds to $\rho_{2D} = 1.8 \times 10^{-5}$ Ωm. Thus λ_c is more than two orders of magnitude smaller than a_0. It is notoriously difficult to measure the in-layer conductivity in strongly anisotropic metals and reported values most probably underestimate $\rho_\parallel$ (Ref. 31). An error of 10^2 or larger is unlikely and the system is most probably a bad metal. At 250 K the conductivity increases under pressure and tends toward a normal metal state, the Ioffe-Regel condition is, however, not yet fulfilled at 1 GPa pressure.

D. Comparison with DMFT theory

In κ-ET$_2$-Cl the metal-insulator transition is the first order below a critical pressure, P_c and a critical temperature,[10] T_c. Above T_c there is a smooth crossover with increasing pressure from a semiconducting to a metallic state. Dynamical mean field theory (DMFT) reproduces qualitatively most observations.[27] The temperature and pressure dependence of the resistivity is assumed to arise entirely from electron correlations characterized by the on-site Coulomb interaction, U and interdimer overlap parameters, $t_{1\parallel}$ and $t_{2\parallel}$ or the bandwidth W. Furthermore, increasing pressure is assumed to decrease the ratio U/W.

At ambient pressure the ground state is insulating, U/W is large, and there are distinct Hubbard bands in the electron spectrum. At higher temperatures the Hubbard bands are smeared but a dip remains in the spectral density and κ-ET$_2$-Cl remains semiconducting. At pressures above P_c a coherent peak appears between the Hubbard bands and the ground state is a normal metal. At pressures just above P_c, the coherent peak broadens with increasing temperature and the system transforms from a normal metal to a semiconductor when excitations of the smeared Hubbard bands become more important than the coherent peak. At somewhat higher pressures, the coherent peak persists and κ-ET$_2$-Cl is a bad metal at high temperatures.

Limelette *et al.*[10] compared the results of the DMFT calculations with the temperature and pressure dependence of the resistivity of κ-ET$_2$-Cl measured at pressures above P_c. They found a good agreement between the experiment and theory. An increase of the bandwidth from 0.35 eV at 0.3 kbar to 0.5 eV at 10 kbar and a constant $U = 0.4$ eV fits well the data. The numerical comparison is restricted to $P > P_c$, where the ground state is metallic.

The comparison of the hopping time, T_x and interplane resistivity, $\rho_\perp$ at 250 K as a function of pressure confirms this picture for $P > P_c$. As shown in Fig. 10, T_x decreases rapidly with pressure, corresponding to the gradual change from a bad metal toward a normal metal. Moreover, the ratio $T_x/\rho_\perp$ decreases with pressure. Equation (5), which is based

on a Fermi liquid picture, applies at pressures well above P_c and the decrease of the DOS by a factor of about 3 from low pressure to 10 kbar is in qualitative agreement with the bandwidth increase suggested by the analysis of Limelette *et al.*[10]

The question remains, however, whether DMFT can describe correctly the observed high temperature crossover with pressure starting from $P < P_c$ (i.e., starting from the insulating side of the Mott transition. At ambient pressure κ-ET$_2$-Cl is semiconducting at all temperatures. At high temperatures, increasing pressure above P_c replaces a dip in the spectral density by a coherent peak at the Fermi level. Although the relation between T_x and $\rho_\perp$ is very different for a semiconductor and a metal, this does not show up in the low pressure $T_x/\rho_\perp$ data. A full theory is lacking, however, and it remains to be seen whether DMFT theory can account for this counterintuitive result.

E. Blocking of the interlayer hopping

Here we discuss the relation of tunneling hopping frequency with parameters of the electronic structure. As noted by Soda *et al.*[32] for the case of quasi-1D metals, the interlayer hopping is described by the Fermi golden rule if the in-plane electron momentum lifetime is long and the motion within the layer is coherent

$$\nu_\perp^{\text{coherent}} = \frac{2\pi}{\hbar} t_\perp^2 g(E_F). \tag{6}$$

Inserting the hopping rates measured in κ-ET$_2$-Br above 50 K (Fig. 7) and the DOS calculated in Ref. 25, we find $t_\perp = 0.06$ meV, apparently in good agreement with low temperature angular magnetoresistance oscillation measurements[4] in a similar compound. However, Eq. (6) cannot account for the temperature dependence of the interlayer resistivity. The strong decrease of $\rho_\perp$ below 50 K is difficult to reconcile with Eq. (6).

To explain a similar dilemma in the cuprate superconductors, Kumar and Jayannavar[24] proposed that the interlayer hopping is blocked by rapid *in-plane* scattering. In their theory, the resistivity anisotropy $\rho_\perp/\rho_\parallel$ is temperature independent. At high temperatures the in-plane motion is incoherent, the in-plane inelastic momentum scattering time τ is much shorter than the characteristic time for tunneling between layers

$$\tau \ll \frac{\hbar}{t_\perp}. \tag{7}$$

Frequent in-plane scattering blocks tunneling by a quantum mechanical effect; electron tunneling from one molecular layer to the next restarts after every in-plane inelastic scattering event. The tunneling rate[24] is "blocked" by a factor of $2\tau/(\hbar/t_\perp)$

$$\nu_\perp = \frac{2t_\perp^2 \tau}{\hbar^2}. \tag{8}$$

Inserting into Eq. (8) a typical value,[4] $\hbar/t_\perp = 10^{-11}$ s, and $\nu_\perp = 1.9 \times 10^8$ s measured in κ-ET$_2$-Br at 250 K, the inelastic scattering time is $\tau = 1 \times 10^{-14}$ s.

According to Eqs. (5) and (8), the *interlayer* conductivity is governed by the *in-plane* scattering time, τ. However, the relation between $\rho_\parallel$ and τ is not simple. It might be tempting to

follow the argument of Ref. 24, and equate τ to the scattering time τ_c defined as

$$\rho_\parallel^{-1} = \frac{ne^2\tau_c}{m^*}, \tag{9}$$

where n is the electron density and m^* is the effective mass. However, in the bad-metal phase Eq. (9) does not hold. From the measured conductivity and assuming an effective mass of the order of the electron mass,[33] m_0, Eq. (9) implies $\tau_c = 10^{-16}$ s (i.e., $\hbar/\tau_c = 7$ eV), an unrealistic value, two orders of magnitude larger than the bandwidth. The inadequacy of Eq. (9) is also clear from its prediction for the resistivity anisotropy. Assuming $\tau = \tau_c$ and using Eqs. (5), (8), and (9)

$$\frac{\rho_\perp}{\rho_\parallel} = \frac{\hbar^2}{2d^2 m^* g(E_F) t_\perp^2}. \tag{10}$$

Although this anisotropy is temperature independent in line with measurements, Eq. (10) predicts $\rho_\perp/\rho_\parallel = 10^5 - 10^6$, a value much larger than the observed $10^2 - 10^3$. Formally, Eqs. (5), (8), (9), and (10) relate T_x, $\rho_\perp$, $\rho_\parallel$, and τ consistently in the bad-metal state, if strong electron correlations at high temperatures are taken into account by a large effective mass of the order of 100 m_0.

F. Two-dimensional spin diffusion

Spin diffusion is two-dimensional in a layered conductor if spin memory of electrons is lost before hopping to the adjacent layer (i.e., if $T_x > T_2$). This is clearly the case in κ-ET$_2$-Cl at ambient pressure and all temperatures (Fig. 9). As a function of pressure, the 2D to 3D crossover at 250 K is at 0.2 GPa (Fig. 5). In κ-ET$_2$-Br the crossover to three-dimensional spin diffusion is at 40 K (Fig. 7).

For possible applications, the 2D spin diffusion length, δ_{eff} in a single layer is important. In normal 2D metals, $\delta_{\text{eff}} = [1/2(v_F^2 \tau_c T_1)]^{1/2}$ is determined by the in-plane momentum scattering time and the spin-lattice relaxation time; in metals usually $T_1 \approx T_2$. In the normal metal phase, the Ioffe-Regel-condition holds at temperatures near T_c, here $\tau_c > 10^{-14}$ s and $\delta_{\text{eff}} > 0.2$ μm. We do not know what the corresponding expression is in the bad-metal phase, where the quasiparticle picture fails. The low conductivity implies that δ_{eff} becomes smaller at high temperatures.

VI. CONCLUSION

We have mapped the interlayer spin hopping time and the intrinsic spin lifetime in the conducting phases of the temperature-pressure phase diagram of κ-ET$_2$-X. Assuming a semiclassical picture where electronic and spin transport are tied together, the temperature dependence of the spin hopping time in κ-ET$_2$-X is proportional to the interlayer resistivity $\rho_\perp$ and the DOS. Typical DOS values from standard band structure calculations[25] are four to five times smaller than the DOS derived from the $T_x/\rho_\perp$ ratio. T_x is roughly proportional to $\rho_\perp$ as the temperature is varied in the semiconductor phase of κ-ET$_2$-Cl, where T_x increases with decreasing T, and also in the bad-metal phase of κ-ET$_2$-Br, where T_x is about constant above 50 K.

In the bad-metal phase the in-plane resistivity is large and the Ioffe-Regel condition is not fulfilled. The resistivity has been calculated in the literature by DMFT theory of a system with comparable on-site Coulomb interactions and bandwidths. The comparison of T_x and $\rho_\perp$ (measured by Weiss *et al.*[22]) under pressure at ambient temperatures in κ-ET$_2$-X tests the theory. The ratio, $T_x/\rho_\perp$ decreases continuously along the crossover between the semiconductor and metal phases. This decrease is in agreement with DMFT on the metallic side of the Mott transition. There is, however, no significant change in the ratio at the lowest pressures where the resistivity changes from semiconducting to bad metal.

We have discussed the relation between the hopping frequency due to tunneling and the band parameters. We note that at high temperatures the in-plane momentum lifetime is much shorter than the coherent tunneling time and the interlayer hopping is blocked by a mechanism suggested by Kumar and Jayannavar.[24] An in-plane inelastic momentum scattering time of $\tau = 10^{-14}$ s is required to understand the interlayer hopping rate in κ-ET$_2$-Br at 250 K by the blocking mechanism. A description based on this scattering time and parameters of the calculated band structure without taking into account electron correlations leads to inconsistent results at high temperatures. Finally, we note that above 50 K spin diffusion is two-dimensional; electrons diffuse to large distances confined within a molecular layer.

*atj@szfki.hu

[1] A. M. Kini, U. Geiser, H. H. Wang, K. D. Carlson, J. M. Williams, W. K. Kwok, K. G. Vandernvoort, J. E. Thompson, D. L. Stupka, D. Jung, and M. H. Whangbo, Inorg. Chem. **29**, 2555 (1990).

[2] J. M. Williams, A. M. Kini, H. H. Wang, K. D. Carlson, U. Geiser, L. K. Montgomery, G. J. Pyrka, D. M. Watkins, J. M. Kommers,

S. J. Boryschuk, A. V. S. Crouch, W. K. Kwok, J. E. Schirber, D. L. Overmyer, D. Jung, and M. H. Whangbo, Inorg. Chem. **29**, 3272 (1990).

[3] A. Fortunelli and A. Painelli, Phys. Rev. B **55**, 16088 (1997).

[4] J. Singleton, P. A. Goddard, A. Ardavan, N. Harrison, S. J. Blundell, J. A. Schlueter, and A. M. Kini, Phys. Rev. Lett. **88**, 037001 (2002).

[5] L. I. Buravov, N. D. Kushch, V. A. Merzhanov, M. Osherov, A. Khomenko, and E. Yagubskii, J. Phys. I (France) **2**, 1257 (1992).

[6] H. Ito, T. Ishiguro, M. Kubota, and G. Saito, J. Phys. Soc. Jpn. **65**, 2987 (1996).

[7] V. N. Zverev, A. I. Manakov, S. S. Khasanov, R. P. Shibaeva, N. D. Kushch, A. V. Kazakova, L. I. Buravov, E. B. Yagubskii, and E. Canadell, Phys. Rev. B **74**, 104504 (2006).

[8] J. J. McGuire, T. Rõom, A. Pronin, T. Timusk, J. A. Schlueter, M. E. Kelly, and A. M. Kini, Phys. Rev. B **64**, 094503 (2001).

[9] S. Lefebvre, P. Wzietek, S. Brown, C. Bourbonnais, D. Jérome, C. Mézière, M. Fourmigué, and P. Batail, Phys. Rev. Lett. **85**, 5420 (2000).

[10] P. Limelette, P. Wzietek, S. Florens, A. Georges, T. A. Costi, C. Pasquier, D. Jérome, C. Mézière, and P. Batail, Phys. Rev. Lett. **91**, 016401 (2003).

[11] F. Kagawa, T. Itou, K. Miyagawa, and K. Kanoda, Phys. Rev. B **69**, 064511 (2004).

[12] K. Miyagawa, A. Kawamoto, Y. Nakazawa, and K. Kanoda, Phys. Rev. Lett. **75**, 1174 (1995).

[13] F. X. Cabanas and C. F. Schwerdtfeger, Phys. Rev. B **39**, 11241 (1989).

[14] A. Antal, T. Fehér, A. Jánossy, E. Tátrai-Szekeres, and F. Fülöp, Phys. Rev. Lett. **102**, 086404 (2009).

[15] A. Antal, T. Fehér, B. Náfrádi, R. Gaál, L. Forró, and A. Jánossy, Physica B: Condensed Matter **405**, S168 (2010).

[16] K. L. Nagy, D. Quintavalle, T. Fehér, and A. Jánossy, Appl. Mag. Resons. **40**, 47 (2011).

[17] B. Náfrádi, R. Gaál, T. Fehér, and L. Forró, J. Magn. Reson. **192**, 265 (2008).

[18] B. Náfrádi, R. Gaál, A. Sienkiewicz, T. Fehér, and L. Forró, J. Magn. Reson. **195**, 206 (2008).

[19] C. Coulon and R. Clerac, Chem. Rev. **104**, 5655 (2004).

[20] T. Nakamura, T. Nobutoki, T. Takahashi, G. Saito, H. Mori, and T. Mori, J. Phys. Soc. Jpn. **63**, 4110 (1994).

[21] B. Náfrádi, A. Olariu, L. Forró, C. Mézière, P. Batail, and A. Jánossy, Phys. Rev. B **81**, 224438 (2010).

[22] H. Weiss, M. V. Kartsovnik, W. Biberacher, E. Steep, E. Balthes, A. G. M. Jansen, K. Andres, and N. D. Kushch, Phys. Rev. B **59**, 12370 (1999).

[23] J. E. Schirber, D. L. Overmyer, K. D. Carlson, J. M. Williams, A. M. Kini, H. H. Wang, H. A. Charlier, B. J. Love, D. M. Watkins, and G. A. Yaconi, Phys. Rev. B **44**, 4666 (1991).

[24] N. Kumar and A. M. Jayannavar, Phys. Rev. B **45**, 5001 (1992).

[25] R. C. Haddon, A. P. Ramirez, and S. H. Glarum, Adv. Mater. **6**, 316 (1994).

[26] C. Strack, C. Akinci, V. Paschenko, B. Wolf, E. Uhrig, W. Assmus, M. Lang, J. Schreuer, L. Wiehl, J. A. Schlueter, J. Wosnitza, D. Schweitzer, J. Müller, and J. Wykhoff, Phys. Rev. B **72**, 054511 (2005).

[27] J. Merino and R. H. McKenzie, Phys. Rev. B **61**, 7996 (2000).

[28] A. Kawamoto, K. Miyagawa, Y. Nakazawa, and K. Kanoda, Phys. Rev. B **52**, 15522 (1995).

[29] N. Yoneyama, T. Sasaki, and N. Kobayashi, Synth. Met. **137**, 1205 (2003).

[30] O. Gunnarsson, M. Calandra, and J. E. Han, Rev. Mod. Phys. **75**, 1085 (2003).

[31] J. Singleton and C. Mielke, Contemp. Phys. **43**, 63 (2002).

[32] G. Soda, D. Jérome, M. Weger, J. M. Fabre, and L. Giral, Solid State Commun. **18**, 1417 (1976).

[33] J. Merino and R. H. McKenzie, Phys. Rev. B **62**, 2416 (2000).